Textures and Microstructures, 1995, Vol. 24, pp.167–197
Reprints available directly from the publisher
Photocopying permitted by license only

TEXTURE AND PROPERTIES OF α–Al_2O_3 SUBSTRATES

A. BÖCKER, H. J. BUNGE, J. HUBER, W. KRAHN and J. RUSKA

Department of Physical Metallurgy, Technical University of Clausthal, Germany, Hoechst CeramTec Selb, Germany

(Received 10 February 1995)

Texture formation in Al_2O_3 substrates after green forming and sintering was studied. The results can be well represented in a texture formation diagram in terms of the green texture and a sintering factor. The sintering factor is related to grain growth. It can be quantified in terms of sintering time and temperatur with a growth rate factor depending on boundary energy and mobility. Two different regions of sintering temperatures can be distinguished of which the high-temperature one is related to liquid phase sintering.
Mechanical properties of the substrates were also studied, particularly thermal cycling fatigue of copper plated substrates as well as thermal shock resistence and bending fracture strength. These properties are influenced in different ways by the texture. The properties can be understood taking also the misorientation distribution of the grain boundaries into account.

KEY WORDS: Al_2O_3, green texture, sinter texture, physical properties, model calculations, texture formation diagram.

INTRODUCTION

Alumina substrates are used in the production of hybride circuits for application, for instance, in the automotive industry, and in telecommunication. They are also used as substrates for resistors and resistor networks in the electronic industry. In these applications they must withstand external mechanical stresses, thermal shock and thermal cycling stresses, the respective properties depending on thermal expansion, elasticity and fracture strength. Furthermore, in some applications the dielectric properties as well as thermal conductivity are of interest. All these properties are anisotropic in the individual crystallites. In a polycrystalline substrate, they may thus also be anisotropic, depending on the orientation distribution of the crystallites, i.e. the texture of the material. Furthermore, microstresses across the grain boundaries may depend on the misorientation of neighbouring grains which is also related to the texture. Hence, it is important to know what kinds of textures occur in alumina substrates, how they influence their properties and how they can be modified in the desired direction. The development of textures in Al_2O_3 ceramics was first studied by Dimarcello *et al.* (1972). Nakada and Schock (1975) attributed textures in Al_2O_3 substrates mainly to the surface region. Our own investigations (Böcker *et al.*, 1991, 1993, 1994) did not confirm this assumption. Hence, it was the purpose of the present investigation to study in more detail how textures are being formed in Al_2O_3 substrates and what their influence on physical properties is.

PRODUCTION OF ALUMINA CERAMICS

Alumina ceramics, similar to most other ceramic materials, are produced by a two-step process i. e. green-forming and sintering. Both these steps allow, however, many variants in detail. Figure 1 shows for instance three of the major variants used in green forming

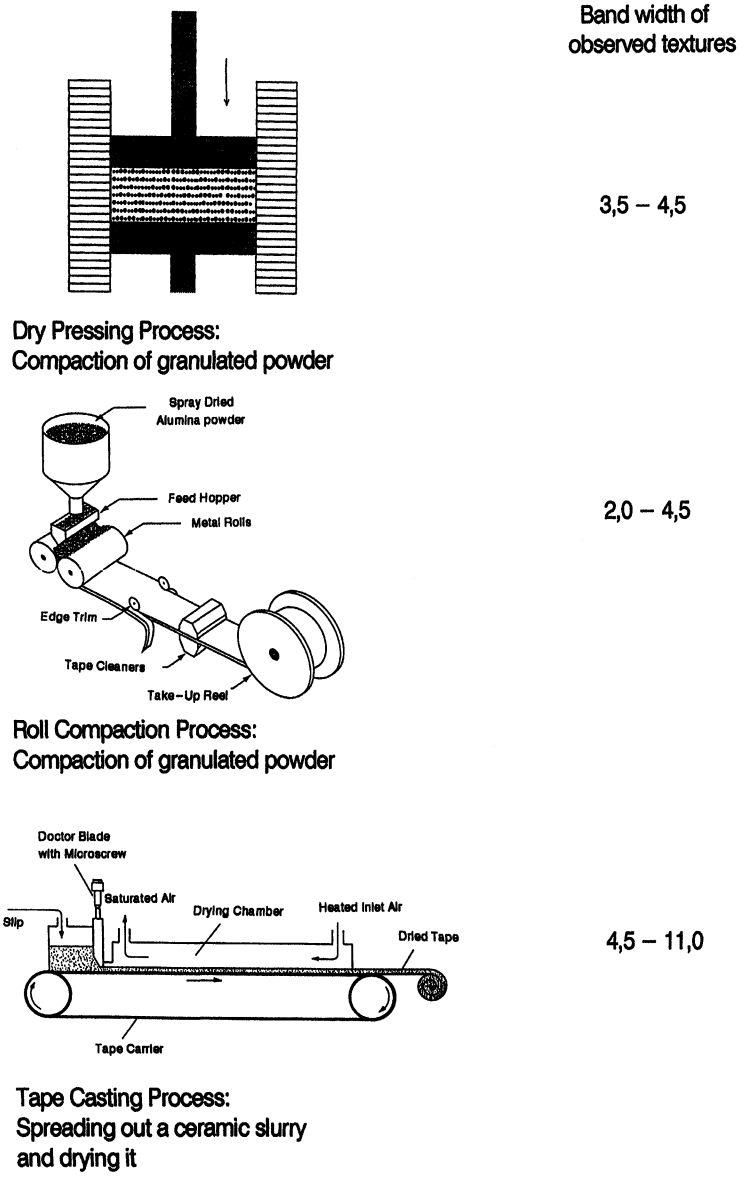

Figure 1 Three major technologies for green forming of Al_2O_3 substrates as well as the bandwith of green textures formed by these processes

of Al_2O_3 substrates i.e. dry pressing, "calandring" i.e. roll compacting, and slurry casting. Each of these processes depends on a large number of influencing parameters as is exemplified in Figure 2 for the particularly important case of slurry casting.

Also the second step, sintering, may be subject to a variety of parameters the most important ones are the time-temperature profile and the atmosphere.

Texture investigations in the present study were mainly done in samples taken out of technological production lines run with different values of the variable parameter within sensitive limits of these parameters. Thus, it was easily possible to take samples after green forming and after sintering. Samples corresponding to intermediate states, i. e. during the green forming process or during sintering were not available, this way. Hence, some additional samples were studied produced in the laboratory by processes imitating the technological processes.

The range of material composition studied in this investigation was similar to that used for the production of "thick-film" and "thin-film" substrates (Table 1).

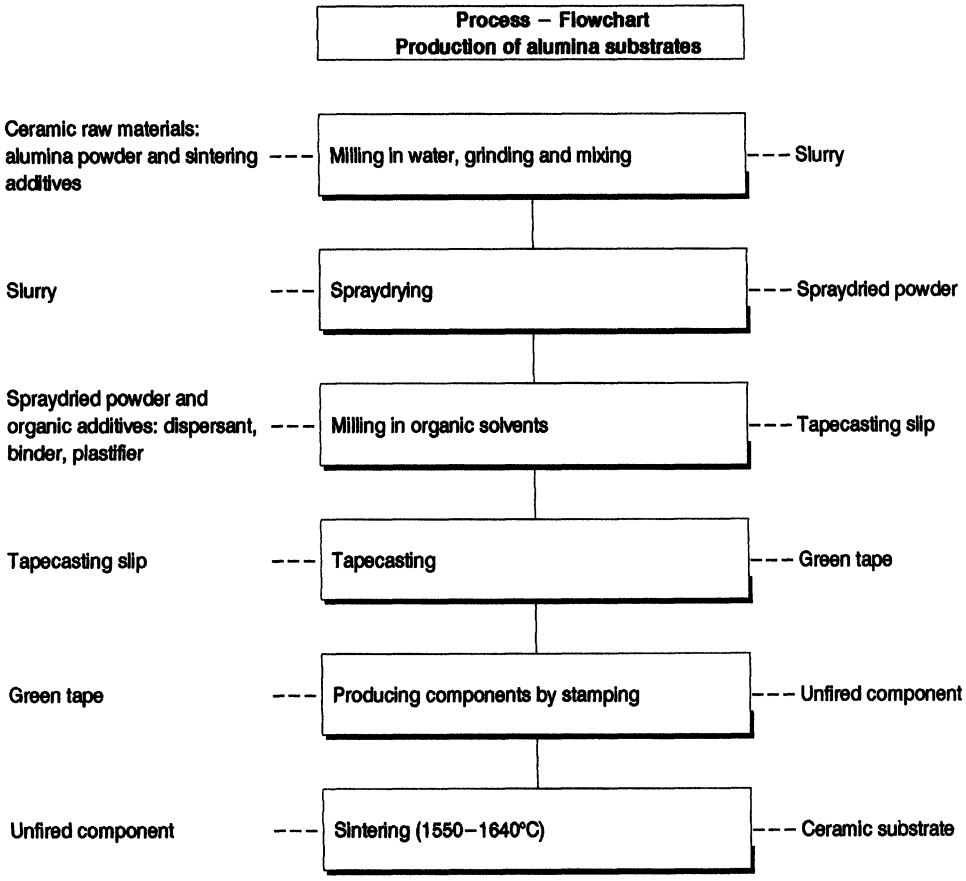

Figure 2 Technological steps in slurry casting

Table 1 Composition range of used materials

Al_2O_3	*Si0*	*Mg0*	*Ca0*	Application
96 % 99.5 %	1.8–3.2	0.5–1.3 ~ 0.5	0.15–0.3	Thick-film Thin-film

METHODS OF TEXTURE INVESTIGATION

Aluminium oxide, α — Al_2O_3 corundum, has a trigonal crystal structure, crystal class $\bar{3}$m with the lattice parameters a = 4.758 Å c = 12.991 Å

For the purpose of texture analysis it has been treated here as hexagonal.

Preliminary texture investigations showed that substrates mostly had textures with the basal plane (0001) parallel to the substrate plane. Also, in most cases there was no preferred orientation in this plane, i.e. the textures were axially symmetric. Hence, the orientation distribution of the basal plane, i.e. the (0001)-pole figure is most important. The basal plane reflections (000*l*) have, however, very low structure factors as is seen in Figure 3a for X-ray diffraction. The relative intensity of the (0006) peak is < 1%. Hence, the direct measurement of this pole figure is very difficult with X-rays. (Though it is not impossible).

Some measurements were carried out in wet slurries using a $\vartheta - \vartheta$-goniometer which allows to keep the surface of the slurry horizontal during measurement. These diffraction spectra were measured with a position sensitive detector, taking measurements in real time while the slurry was drying.

As is seen in Figure 3b, the structure factor of the (0006) plane is much higher for neutron diffraction. Hence, neutron diffraction can be used for direct measurement of basal plane pole figures (Böcker *et al.*, 1991).

In the case of X-ray diffraction, other diffraction peaks have much higher relative intensities. Hence, it is more appropriate to measure the pole figures of these peaks, to calculate the ODF, and then to calculate the basal plane pole figure. This method has been mainly used in the present investigation. Particularly, the pole figures listed in Table 2 were measured.

The obtained ODF could be well represented by the preferred orientation $g = \{\varphi_1, 0, 0\}$ $0 \leq \varphi_1 < 360°$ i.e. the basal plane parallel to the substrate plane with spread about it according to a Gauss distribution with respect to Φ

$$f(g) = f_{max} \cdot e^{-\left(\frac{\Phi}{\omega}\right)^2} ; \; g = \{\varphi_1 \Phi \varphi_2\} \tag{1}$$

where ω is the spread width. Hence, spread width ω and maximum density f_{max} are correlated to each other (Böcker *et al.*, 1994). This particular type of texture can thus be characterized by one parameter, i.e. either f_{max} or ω. In the present study we used f_{max} as the characteristic parameter. The random orientation is then characterized by

$$f_{max} = 1 \qquad \text{random.} \tag{2}$$

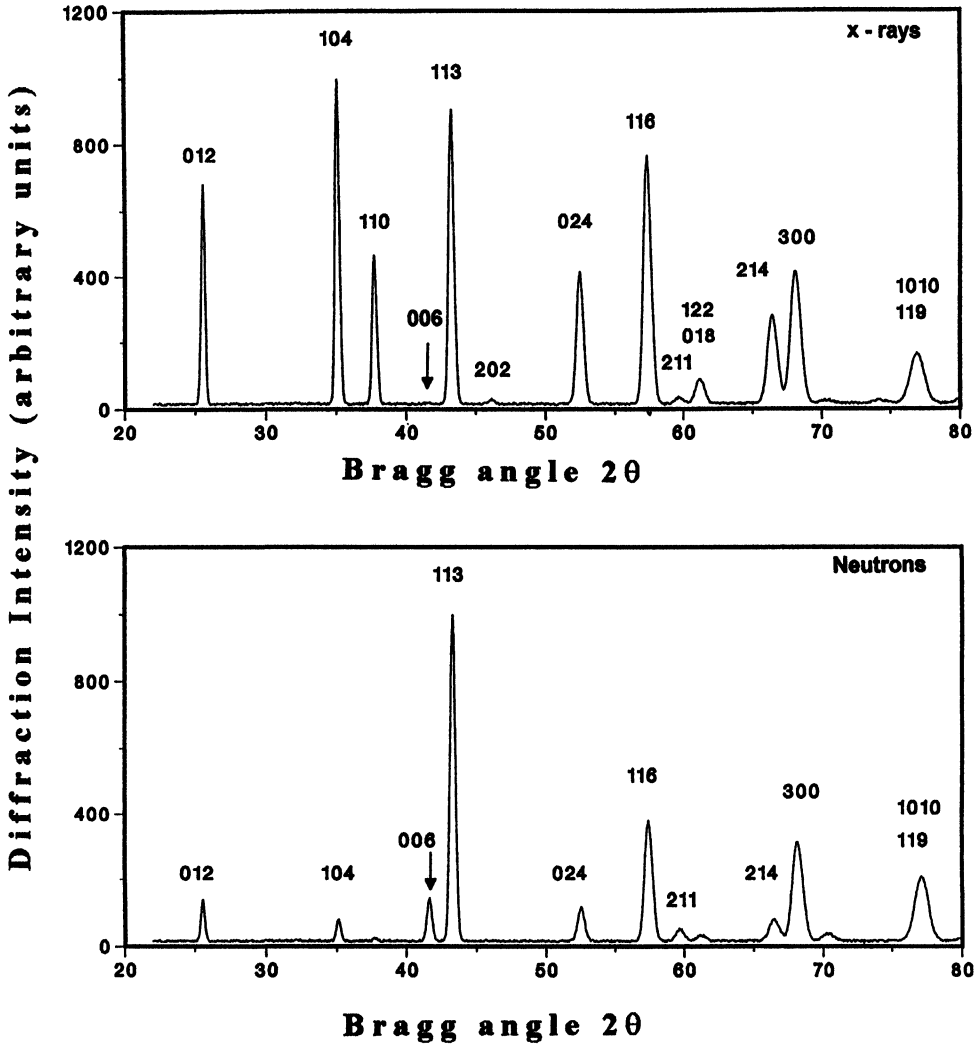

Figure 3 Calculated diffraction diagrams of random Al_2O_3 samples a) X-ray diffraction b) neutron diffraction

Table 2 Pole figures used for texture analysis and their relative intensities

Pole figure	$(10\bar{1}4)$	$(02\bar{2}4)$	$(11\bar{2}6)$	$(11\bar{2}3)$
relative intensity	100%	45%	80%	90%

In models of texture formation it is convenient to have a texture parameter which is zero in the case of random distribution. Hence, the "texture strength" factor

$$\varphi = f_{max} - 1 \tag{3}$$

was introduced which is zero in the case of random distribution.

RESULTS OF TEXTURE INVESTIGATION

Influence of green forming

The influence of the green forming technology on the final texture i.e. after sintering, was already estimated in Figure 1. In this figure the band width of textures observed under usual production conditions is shown. It is seen that by slurry casting the greatest variation range as well as the absolutely highest textures were observed. Hence, in the following, particularly this technology was studied in more detail. The band widths in Figure 1 were observed by variation of the production parameters within the usual limits. Keeping the parameters constant keeps also the variation range of the observed textures within much narrower ranges as is shown in Figure 4.

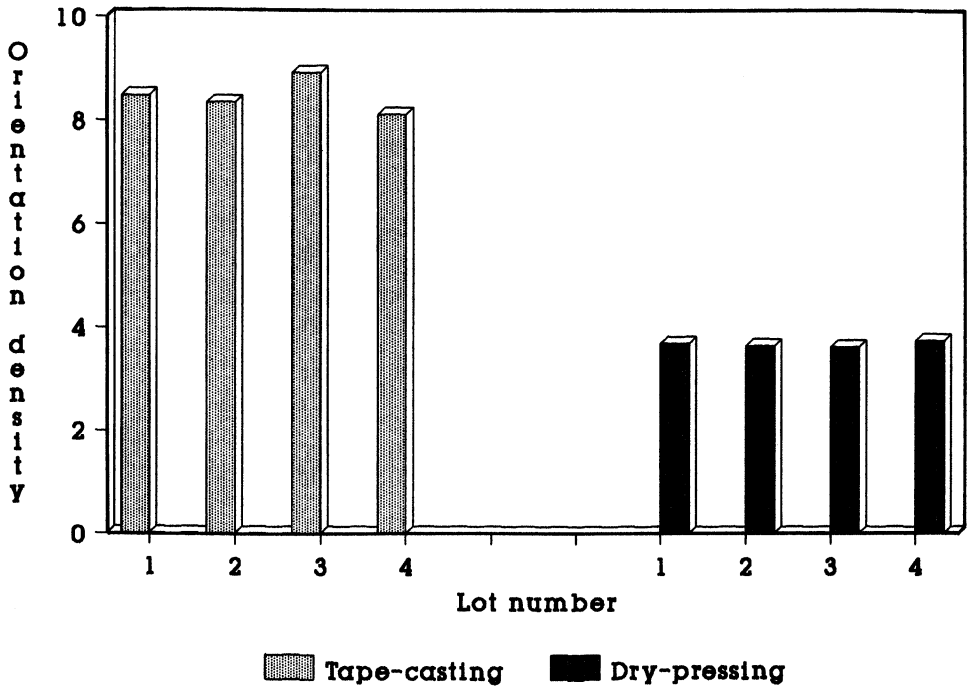

Figure 4 Maximum orientation densities in substrates produced by slurry casting and dry pressing under nominally constant conditions

Texture formation starts with the texture formed in the green body, which is then modified by sintering. It turned out that sintering always increased the texture (at least in all studied cases). Hence, the green texture is the most important first step. Figure 5 shows basal plane pole figures obtained by slurry casting in laboratory tests and by dry pressing. Slurry casting leads to the strongest texture when the slurry is streaked out unidirectionally. Pouring a slurry (without streaking) onto a substrate results in a somewhat weaker texture. These differences may be easily understood. Green textures are formed by rigid particle rotation which is more difficult in a dry aggregate of particles than in a slurry. Furthermore, in the slurry two physical processes must be taken into consideration i.e. surface tension and shear flow. Hence, the stronger texture of the streaked sample can be understood.

The textures in Figure 5 were measured after the foils were dried. Texture formation was, however, observed immediately after the slurry was poured out i.e. in the wet state. The following drying did virtually not change the orientation of the basal plane as is seen in Figure 6a. Texture formation could be correlated to the formation of a dried skin on the surface of the slurry. When skin formation was suppressed e.g. by covering the surface by a thin transparent mylar foil, then the basal plane reflex (0006) was not observed Figure 6b).

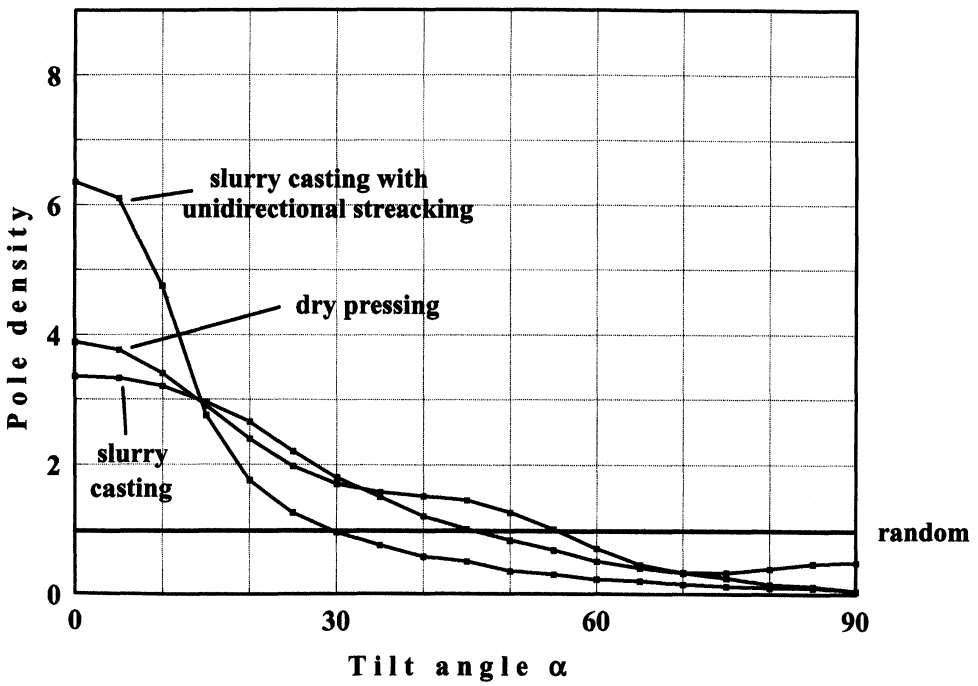

Figure 5 Pole density distributions (0006) of green bodies obtained in three different ways a) dry pressing b) slurry casting c) slurry casting with unidirectional streacking

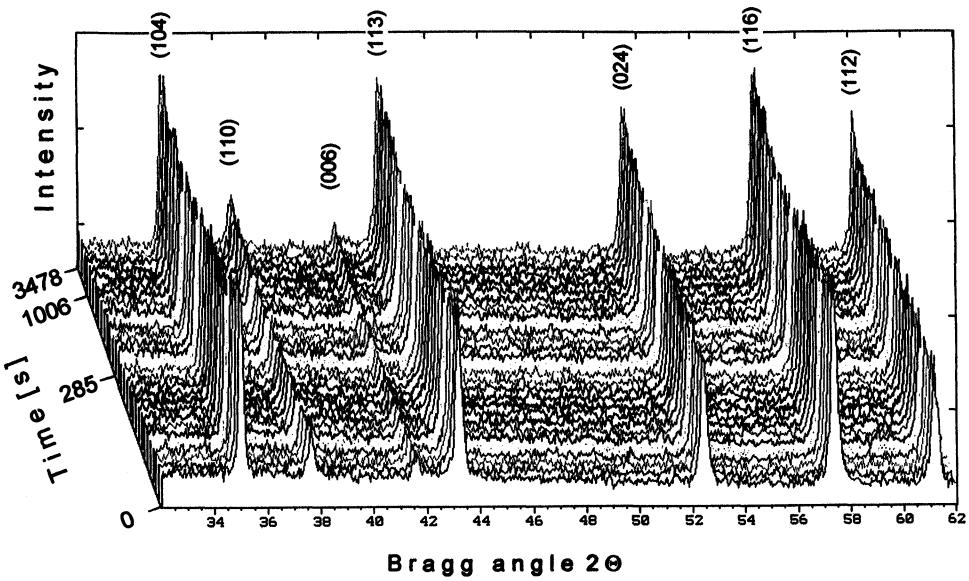

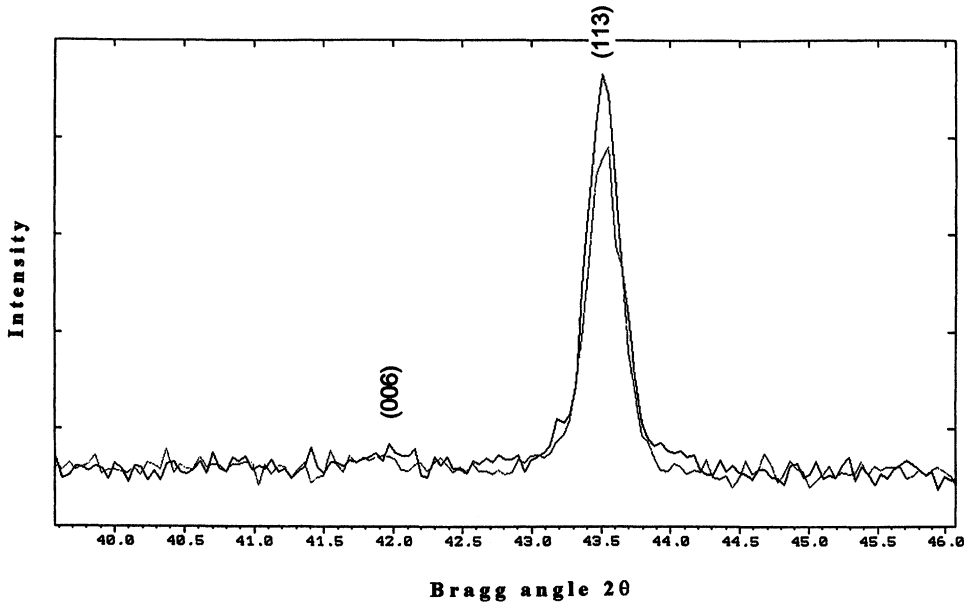

Figure 6 Real time diffraction diagrams obtained immediately after slurry pouring and during drying a) with a free surface b) covered with a mylar foil

Influence of sintering

Sintering was carried out in air under normal pressure. Hence, the essential parameters were sintering time and temperature or, more precisely, the total time-temperature regime. In order to study the influence of sintering time and temperature the regimes shown in Figure 7a, b were used.

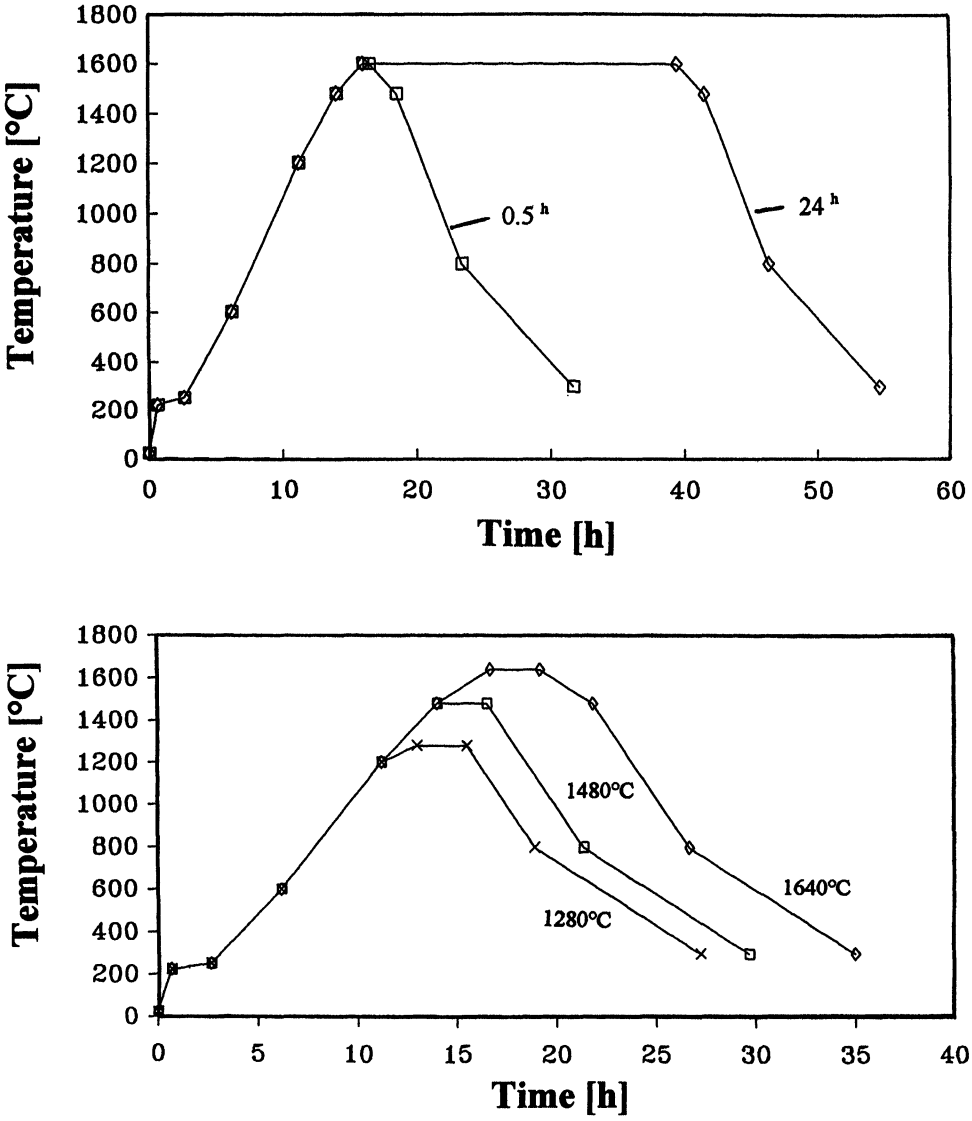

Figure 7 Heating-cooling regimes in the sintering process a) Variation of sintering time, i.e. time at peak temperature b) Variation of peak temperature

Figure 8 shows the time dependence of the final texture at 1600°C for two different materials. It is seen that in both cases the curves are nearly parabolic but with different rate constants in different materials.

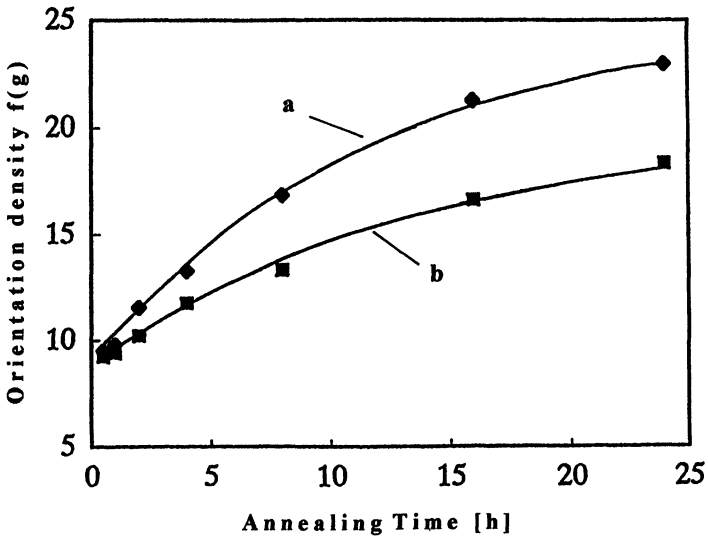

Figure 8 Time dependence of the final sintering texture at T = 1600°C peak temperature a) Powder Cl 3000 b) 10% powder A14, 33% powder Cl3000, 57% powder C75RG

Figure 9 shows the temperature dependence at constant time, i.e. 2.5 hours. It is seen that in both cases the shapes of the curves are similar, but again they have different rate constants (and also different starting textures).

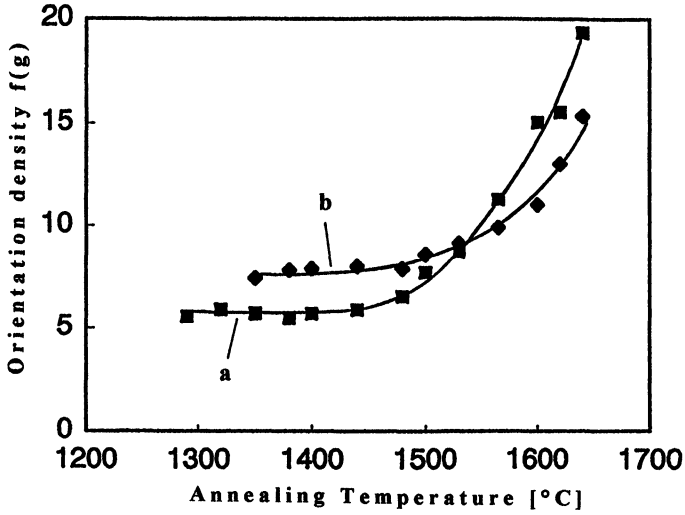

Figure 9 Temperature dependence of the final sintering texture for peak times of 2.5^h a) Powder size 1.2–1.7μm b) Weight ratio powder A / powder B = 1 : 8.5

The increase of the texture strength was always correlated with an increase of grain size. Figure 10 shows, for instance, the grain structure of the same substrate after 0.5^h and 24^h respectively at 1600°C. Finally, Figure 11 shows the correlation of grain size and texture strength during sintering at 1600°C after 0.5^h and 24^h, respectively, for three different materials. It is seen that the tendency is the same in all cases but the growth rates as well as the final textures and final grain sizes are different in different materials.

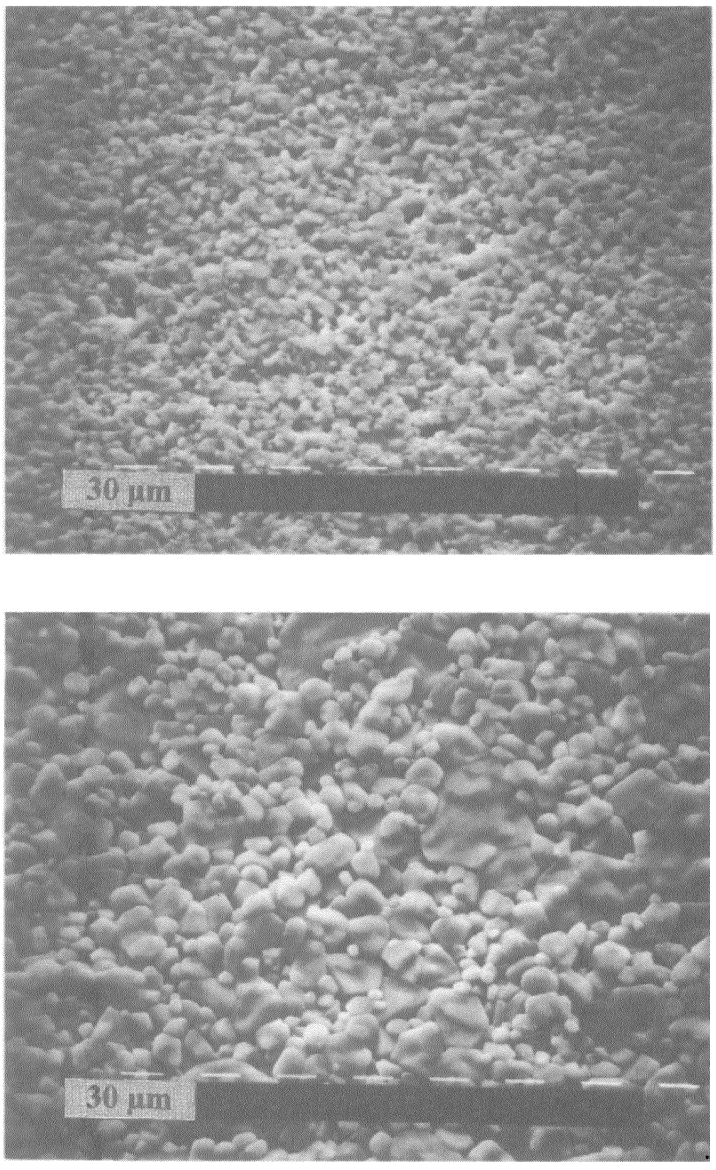

Figure 10 Grain structures of the same substrate after sintering at 1600°C a) after 0.5^h b) after 24^h

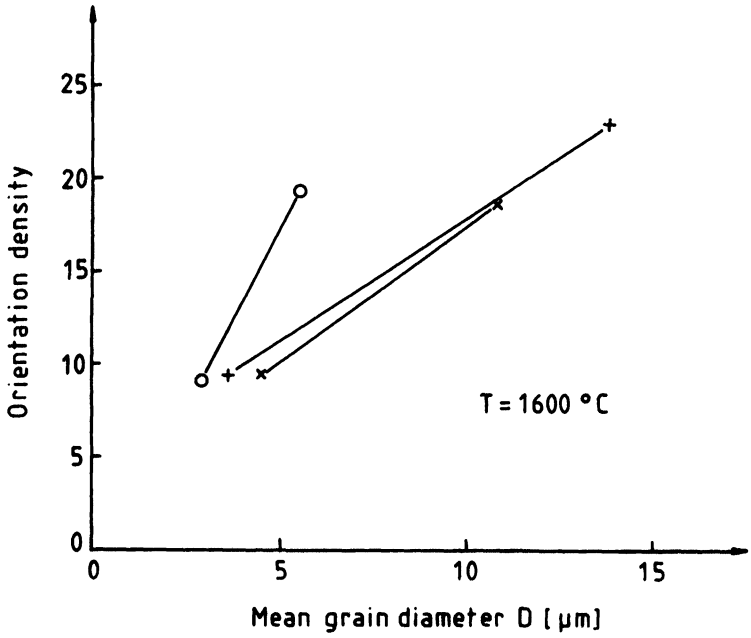

Figure 11 Correlation of grain size and texture strength during sintering at 1600°*C* from 0.5^h to 24^h in three different materials

If it is assumed that the increase of texture is due to continuous grain growth during sintering then time and temperature laws for texture development should be similar to those observed in continuous grain growth, the essential parameters being activation energy of grain boundary mobility and driving force due to the total grain boundary area(see e.g. Bunge and Dahlem-Klein 1993). With these assumptions the following model equation is obtained (Böcker *et al.*, 1994)

$$\varphi^{Sinter} = \varphi^{Green} \cdot q\left[1 + a \cdot \gamma \cdot m \cdot p \cdot e^{-\frac{Q}{RT}} \cdot \sqrt{\frac{t}{t_s}}\right] \tag{4}$$

with

t_s = some standard sintering time (e.g. 2.5^h)
γ = specific grain boundary energy
q = a numerical factor near unity describing some slight texture changes during the initial stages of sintering
m = grain boundary mobility
Q = activation energy of boundary mobility
a = total grain boundary area per unit volume
p = a microstructural parameter depending on the orientation-size distribution, illustrated in Figure 23. It relates grain growth to "texture growth" and has the dimension of an inverse velocity

The total boundary area a per unit volume is related to grain size distribution $n(r)$ by

$$a = \frac{1}{6}\frac{\int r^2 \cdot n(r)dr}{\int r^3 \cdot n(r)dr} \tag{5}$$

(Assuming equiaxed grains)
Also, it is useful to define a "sintering factor" S for "standard" sintering conditions (e.g. $T_s = 1600°C$, $t_s = 2.5^h$)

$$S = \varphi\ (T_s,\ t_s)/\varphi_0\ ;\ \varphi_0 = q \cdot \varphi^{\text{Green}} \tag{6}$$

This factor characterizes the sintering properties of a material. With eq(4) it depends essentially on the dimensionless product $a \cdot \gamma \cdot m \cdot p$ (as well as on the activation energy)

$$S = 1 + a \cdot \gamma \cdot m \cdot p \cdot e^{-\frac{Q}{RT_s}}. \tag{7}$$

The time dependence described in eq(4) can be easily proved by plotting the texture values over $\sqrt{t}$ as is done in a particular example in Figure 12. The temperature dependence is best represented in an Arrhenius plot as is shown in Figure 13 a for another particular example.

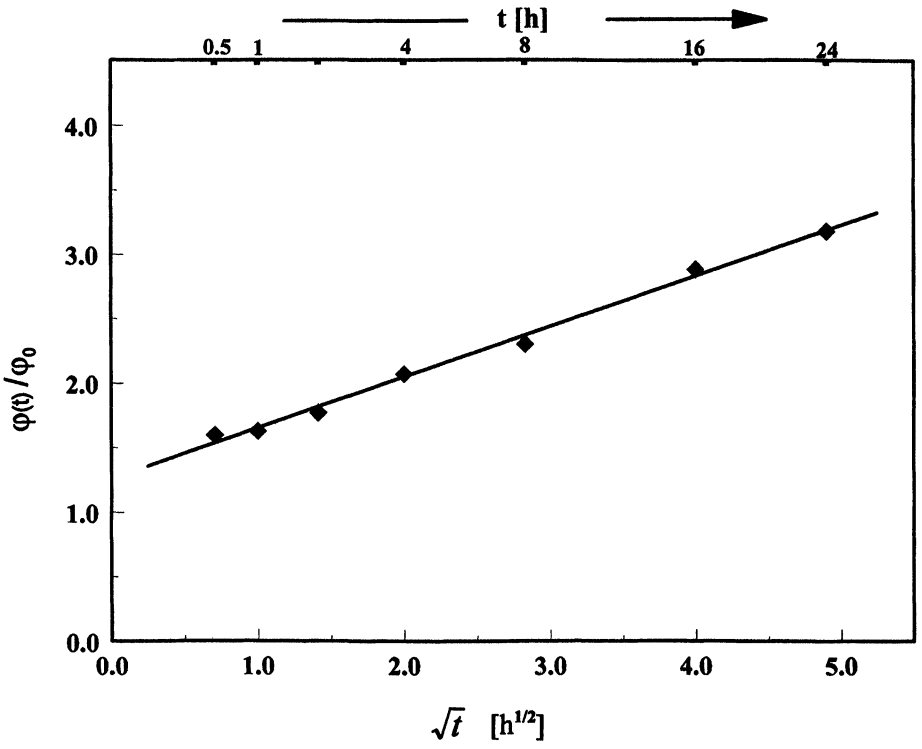

Figure 12 The time dependence of the texture strength at 1600°C plotted as a function of $t^{1/2}$

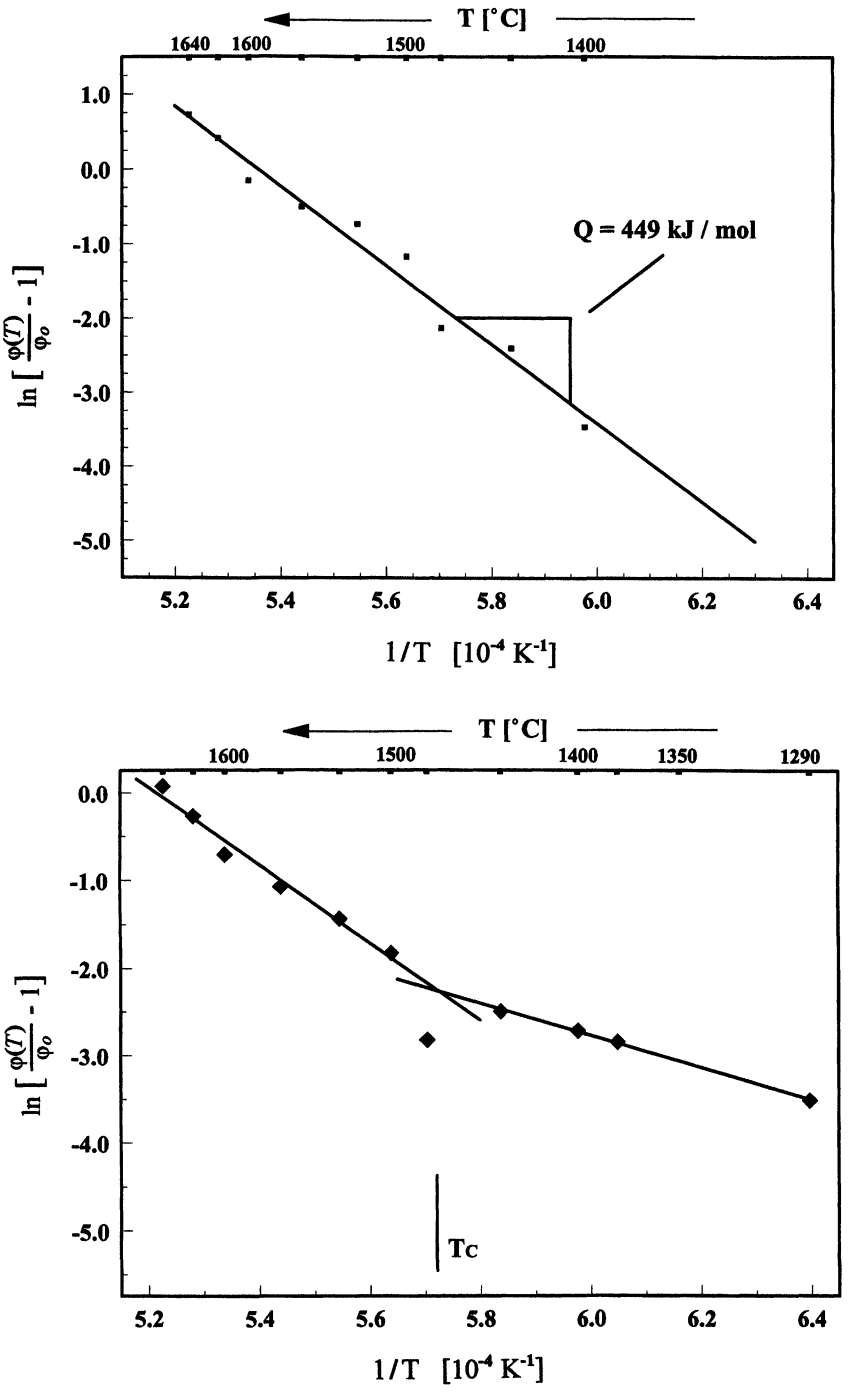

Figutre 13 The temperature dependence of the texture strength after 2.5^h represented in an Arrhenius plot a) Sample showing one Arrhenius line b) Sample showing two Arrhenius lines

In some cases it was found that eq(4) did not hold in the whole temperature range with only one activation energy. Rather two activation energies were needed (Böcker 1994)

$$Q = Q_{high} \text{ for } T > Tc$$
$$Q = Q_{low}, \text{ for } T < Tc \quad (8)$$

It must, however, be mentioned that the values of Q_{low} depend on the small difference $\varphi - \varphi_0$ which can only be obtained with sufficient accuracy when very accurate texture measurements under completely identical conditions are available. Hence, Q_{low} was only evaluated in a few cases. Nevertheless, it seemed, however, possible to estimate Tc even in some cases were Q_{low} could not be evaluated. The results obtained in a variety of different materials are summarized in Table 3. (The sintering factor S always corresponds to the high-temperature range).

Influence of the material and its pretreatment

In Table 4 the influence of a large number of technological parameters on the green texture and the final sintering texture is shown. The table contains the maximum and minimum values observed in a variety of cases. In order to estimate the influence of

Table 3 Quantities obtained from Arrhenius plots of several materials

Material	Activation energy [KJ / mol]		Critcal temperature [°C]	Sinter factor	
	$T > Tc$	$T < Tc$	Tc	S	$a \cdot \gamma \cdot m \cdot p$
1	438			2.35	$2.20 \cdot 10^{12}$
2	375	215	1454	1.57	$1.64 \cdot 10^{10}$
3	482			1.81	$2.24 \cdot 10^{13}$
4	403		1408	3.29	$3.97 \cdot 10^{11}$
5	449			2.78	$5.91 \cdot 10^{12}$

Table 4 Band widths of green and sinter textures by varying several technological parameters

	Green texture			Sintering texture		
	from	to	Band width	from	to	Band width
Kind of raw alumina	1.9	8.2	6.3	3.1	12.6	9.5
Sintering aids	4.6	6.2	1.6	8.6	10.1	1.5
Binder	6.3	7.0	0.7	10.5	11.5	1.0
Solvent	5.5	6.3	0.8	8.6	10.6	2.0
Softener	7.0	7.7	0.7	12.0	13.4	1.4
Raw material processing	5.0	5.4	0.4	10.4	14.1	3.7
Slurry drying	6.9	7.2	0.3	12.2	12.4	0.2
Slurry caster	4.6	5.2	0.6	8.8	9.9	1.1
Tape thickness	6.8	7.2	0.4	11.3	12.3	1.0
Subsequent mechanical compaction	6.3	6.7	0.4	9.4	10.0	0.6

one parameter the other ones were varied in "sensible limits". Hence, the band width given in this table corresponds to the "projection" of the variability due to the whole parameter field onto the considered one. In this way the influence of the individual parameter is somewhat "blurred out" but nevertheless it gives a good survey of the order of magnitude to be expected from the different parameters.

It is seen that the kind of the used alumina raw materials has the greatest influence on the green texture as well as on the sintering texture.

As a second influencing parameter, the processing of the raw material can also be identified. This parameter influences mainly the sintering texture while its influence on the green texture is smaller.

Considering the results obtained according to green texture formation, it may be assumed that particle *shape* has a great influence on this texture. Considering eq(4)(5) a great influence of particle *size* distribution must be expected during grain growth.

In order to better distinguish the two influencing factors, green texture and sintering factor were plotted for several raw materials in Figure 14. It is seen that the type of the material has a great influence on both factors. Figure 14 also gives the product of both factors i.e. the final texture φ^{sinter}. (It must be kept in mind that the sinter factor is defined for "standard" sintering conditions. Hence, the sinter texture in Figure 14 is a "standard" sinter texture. If other sintering conditions, i.e. T and t are used then the actual sintering texture may be different from that "standard" sinter texture).

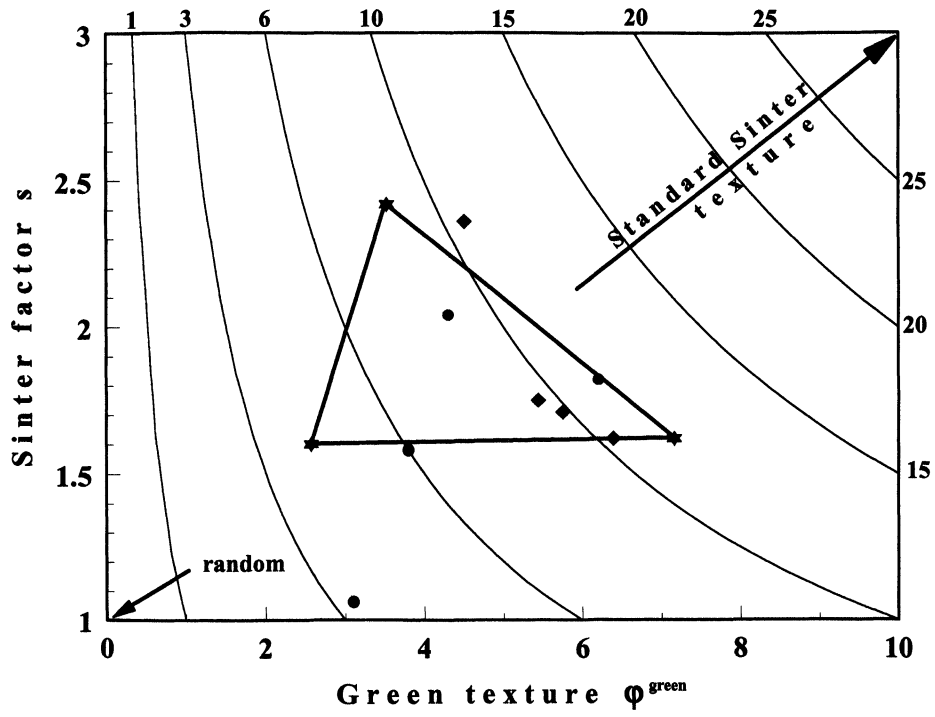

Figure 14 Green textures and sintering factor for different raw materials as well as mixtures of these * three basic powders ◇ mixtures of the basic powders • further powders

Figure 14 also contains the corresponding values obtained with mixtures of several raw materials. It is seen that the representive points of these mixtures in Figure 14 follow roughly the linear mixture rule

$$\{S,\ \varphi\}_{mixt} = \sum_i V_i\ \{S,\ \varphi\}_i \tag{9}$$

where V_i, are the weight fractions of the materials i.
In Figure 15 the influence of several material pretreatments is given. These treatments were undertaken with the purpose of obtaining finer particle sizes. It is seen that in all cases the representing point $\{S,\ \varphi\}$ moves in the direction of a higher sintering factor whereas the green texture remained essentially unchanged. This is in agreement with the results of Table 4 which showed already that materials treatment has a significant influence on the sinter texture but only a small influence on the green texture.

In Table 4 also other parameters showed some influence, but to a much lesser extend so that we shall restrict ourselves here to these two major influences. Figure 16 summarizes schematically the observed texture formation in the production process based on slurry casting.

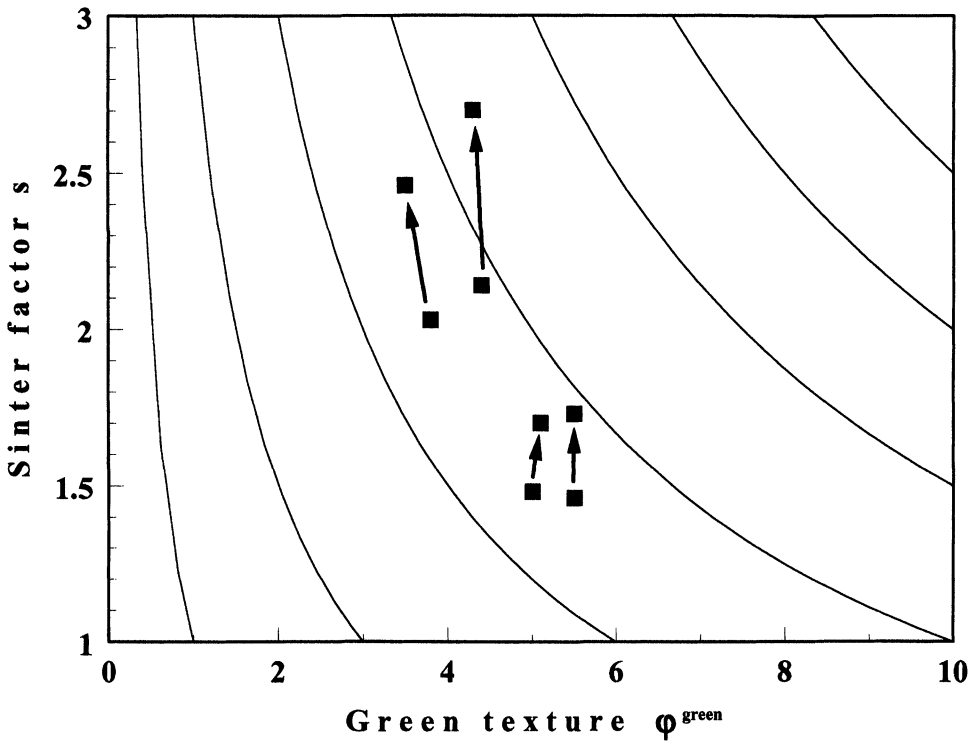

Figure 15 Changes of green texture and sintering factor by materials processing of four different materials. The arrows indicate materials processing towards finer powders

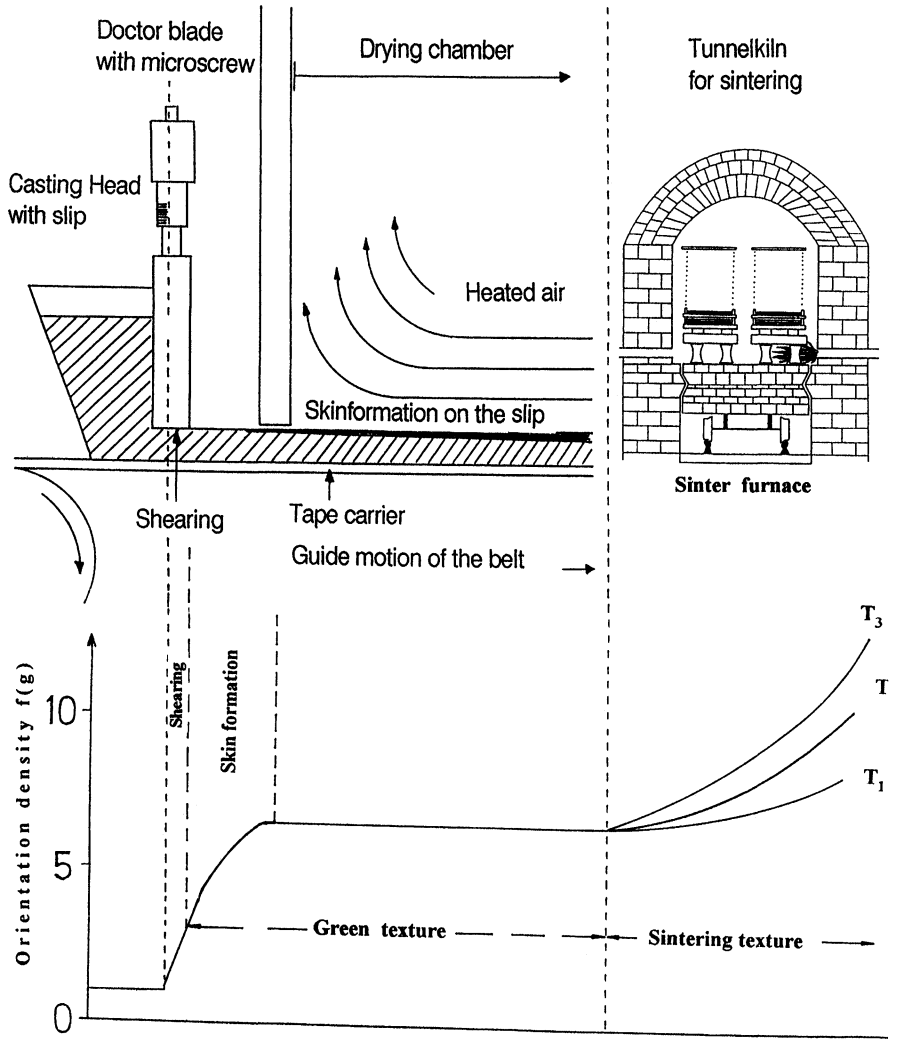

Figure 16 Development of the texture in the production process of Al_2O_3 substrates (schematic)

Physical properties of the substrates

The first physical property tested in the substrates was thermal cycling resistance of copper plated substrates (Klein et al 1989). Such plated substrates were cycled between –40°*C* and +110°*C*. Because of the difference in thermal expansion between copper and alumina this introduces shear stresses in the substrate which finally breaks with an interiour fracture plane parallel to the substrate plane (not at the interface between copper and alumina). The number of cycles that a substrate could withstand befor breaking is plotted in Figure 17 versus f_{max}. It is seen that there is a strong correlation between texture strength and thermal cycling resistance.

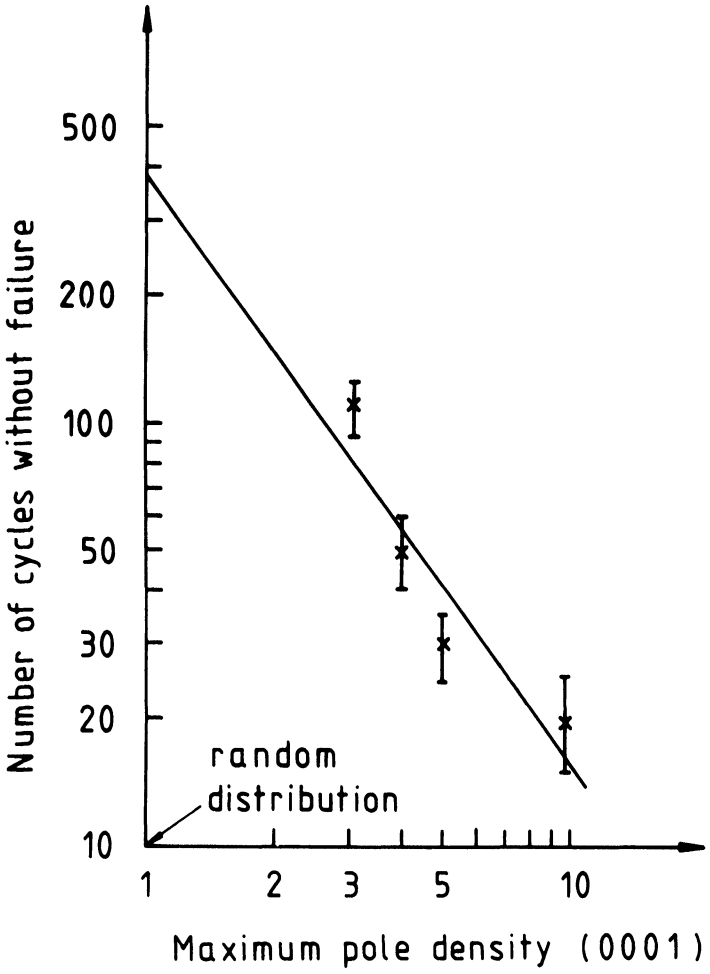

Figure 17 Resistance to thermal cycling of copper plated substrates

A second tested property was fracture strength in a bending test. The results are shown in Figure 18. There seems to be a slight dependence of fracture strength on the texture strength. This is, however, well within the limits of experimental scatter.

A third test was thermal shock resistance. For this test substrates (not plated) were inserted four times into a liquid solder alloy Pb-Sn at 315°C. Figure 19 shows the failure rate of substrates after this test. Although this is a test with great statistical scattering, a tendency can be recognized in Figure 19 shown by the line which markes the onset of sample failure. It is seen that substrates with a strong texture have, in the average, a higher survival rate than those nearer to random orientation distribution. Comparing these three mechanical tests we find an increase, nearly independence, and a decrease of the corresponding property with increase texture strength. This is, however, not contradictory.

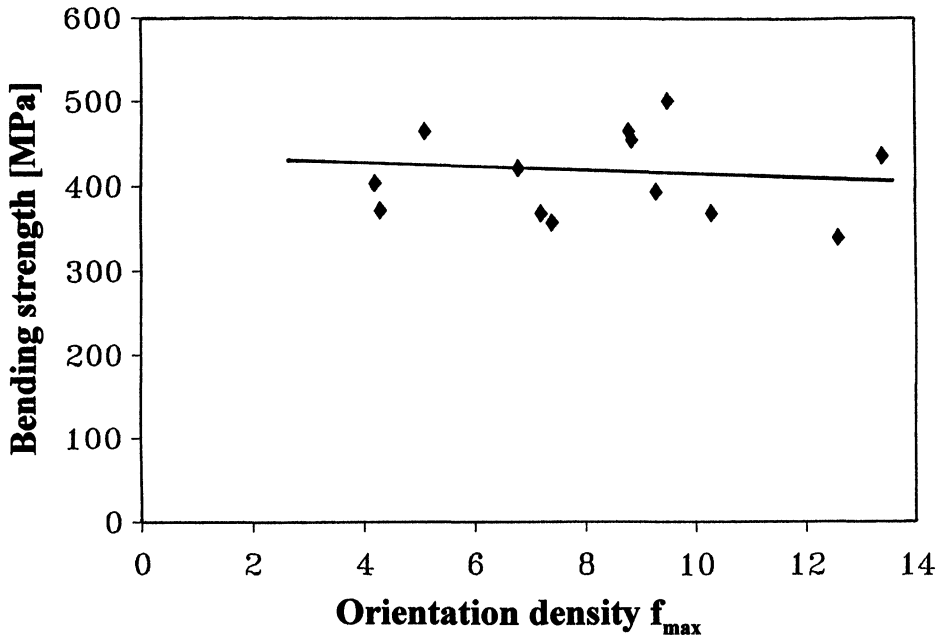

Figure 18 Fracture strength of substrates in a bending test

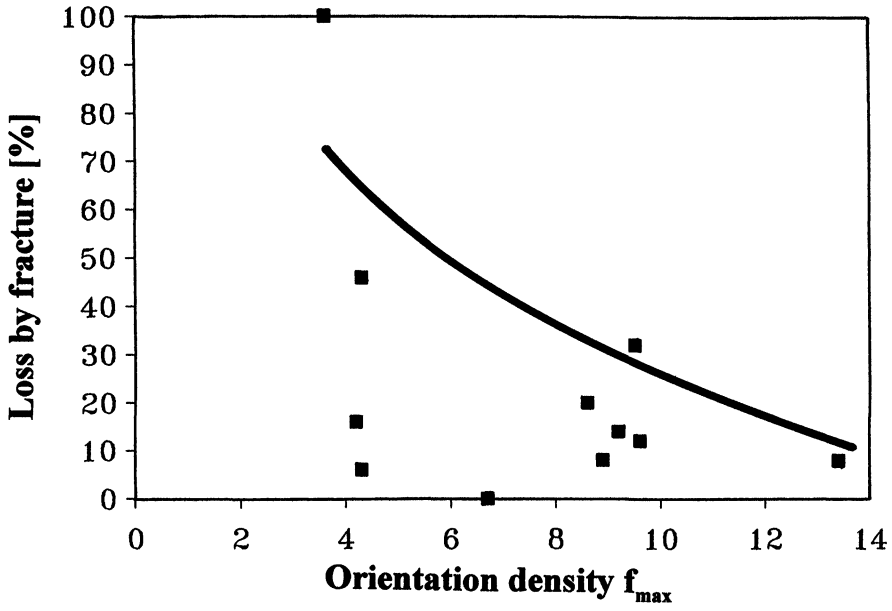

Figure 19 Failure probability of substrates of different texture strength after thermal shock tests. The points are the loss ratios measured in an individual test series. The curve markes roughly the expected loss ratio

The strong decrease of thermal cycling resistance of copper plated substrates was attributed to shear stresses with the shear plane parallel to the substrate plane as a result of different thermal expansion of copper and alumina (Klein *et al* 1989). This was corroborated earlier by the experimental fact that the resistance was lower with thicker copper plates and hence higher shear stresses. The texture dependence was attributed to the cooperation of two effects illustrated in Figure 20.

- Thermal expansion of alumina is anisotropic. Hence, the macroscopic value in the substrate plane is texture-dependent (see e.g. the model calculations Figure 21). As is illustrated in Figure 20, this leads to a slightly smaller difference in expansion in the random material compared to textured material and hence to smaller shear stresses in the random material. The difference in thermal shear stresses according to this effect was estimated to be in the order of magnitude of 9% between textured and random material
- Independent investigations had shown that the expected lifetime in cyclic bending tests (i.e. the number of cycles N till to failure) depends very strongly on the applied stress. It was found (Waibel *et al.*, 1990)

$$N = const \cdot \sigma^{-n} \quad n \approx 24 \tag{10}$$

  Similar results were also obtained by Winkelmann *et al.* (1994). With a difference of 9% in the stresses this leads already to a factor of 2 in the number of cycles, for textured and random material
- Furthermore, the cleavage plane of Al_2O_3 is the basal plane. Hence, in strongly textured samples a continuous crack-path may be developed as is illustrated in Figure 20 whereas in random material the crack path is stopped at the grain boundaries of neighbouring crystallites. Hence, a higher stress in textured materials also finds a lower stress resistance which explaines the strong texture dependence in Figure 17. This second factor may also be expressed in terms of the misorientation distribution MODF of the crystallites which is related to the texture.

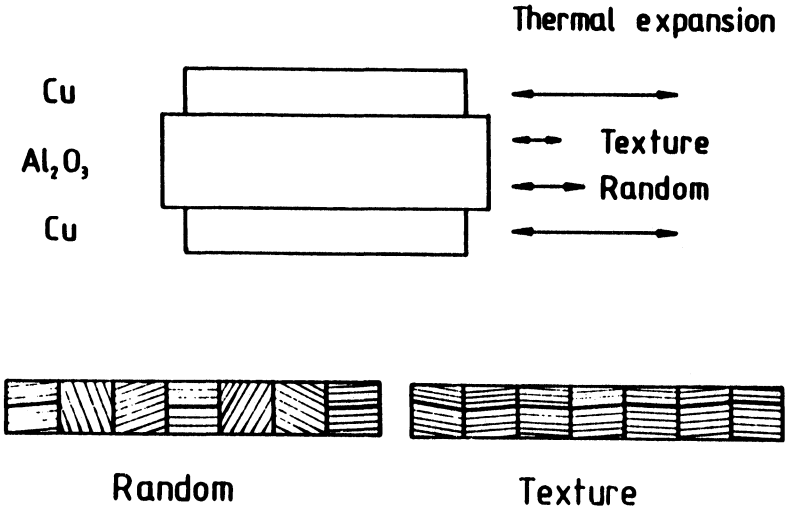

Figure 20 Thermal shear stresses in copper bonded Al_2O_3 substrates due to different expansion coefficients and fracture resistence as a function of grain misorientation

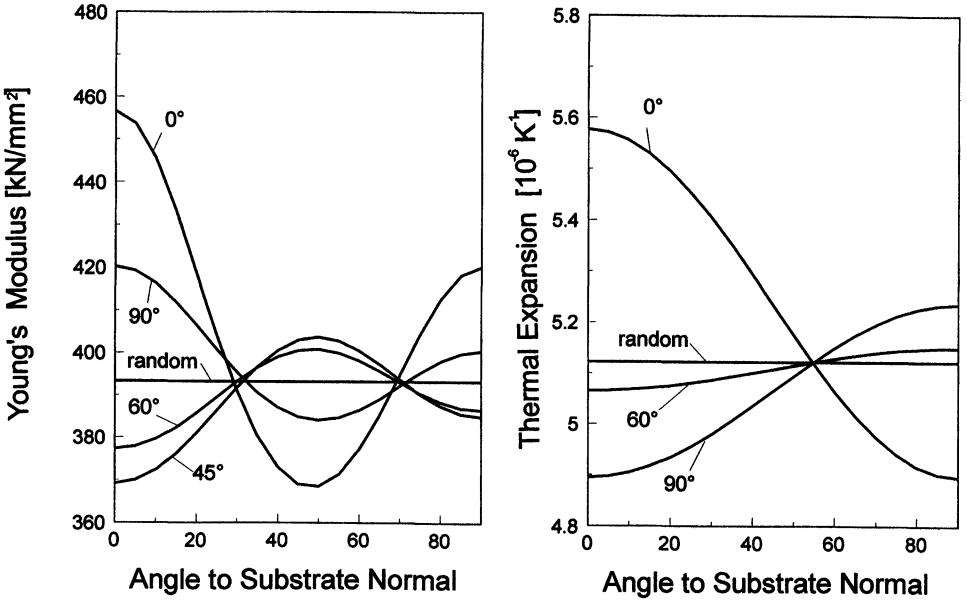

Figure 21 Second and fourth-rank properties of Al_2O_3 assuming different model textures 1) Basal texture $\{\varphi_1, 0°, \varphi_2\}$, $\omega = 0°$ 2) Axial texture $\{\varphi_1, 90°, \varphi_2\}$, $\omega = 0°$ 3) Conical textures $\{\varphi_1, 45°, \varphi_2\}$, $\{\varphi_1, 60°, \varphi_2\}$, $\omega = 0°$ 4) Random distribution a) Young's modulus b) thermal expansion

The situation is quite different for the thermal shock test in Figure 19. Instead of macro-stresses (stresses of 1st-kind) in the copper plated substrates, here microstresses (stresses of 2nd-kind) due to anisotropic thermal expansion of neighbouring crystallites must be considered. Assuming thermal expansion coefficients of $\alpha_{\parallel} = 6.9$ and $\alpha_{\perp} = 5.5$ in the basal plane and c-axis respectively, a discontinuity of thermal expansion accross a grain boundary of up to 22% may occur, depending on the particular misorientation accross this particular boundary. This introduces stresses in the grains which are the stronger the stronger the misorientation, and that in turn *increases* with *decreasing* texture strength. This effect is assumed to be the explanation for the increasing survival rate in Figure 19 with increasing texture strength. According to this model the strongest stresses are to be expected in the vicinity of the grain boundaries. Hence, the fracture strength of the boundaries is an important factor for the fracture strength of the material as a whole. In Figure 19 samples from different charges are plotted in the same diagram. It must be assumed that they have different grain boundary properties such as for instance, different amounts of glass phase. This effect may be responsible for the large spread of the values in this diagram.

Finally, in the bending test in Figure 18, again macrostresses (stresses of 1st-kind) are introduced. These are, however, mainly normal stresses rather than shear stresses as in copper plated substrates. It is shown in the model calculations Figure 22 that a stronger texture leads to a higher Youngs's modulus in the substrate plane and hence to higher stresses at the same bending radius. The difference of stresses due to this effect is in the order of 3%. Contrary to cyclic fatigue resistance, in this essentially static test, a linear dependence of failure on stress must be assumed. Hence, this model

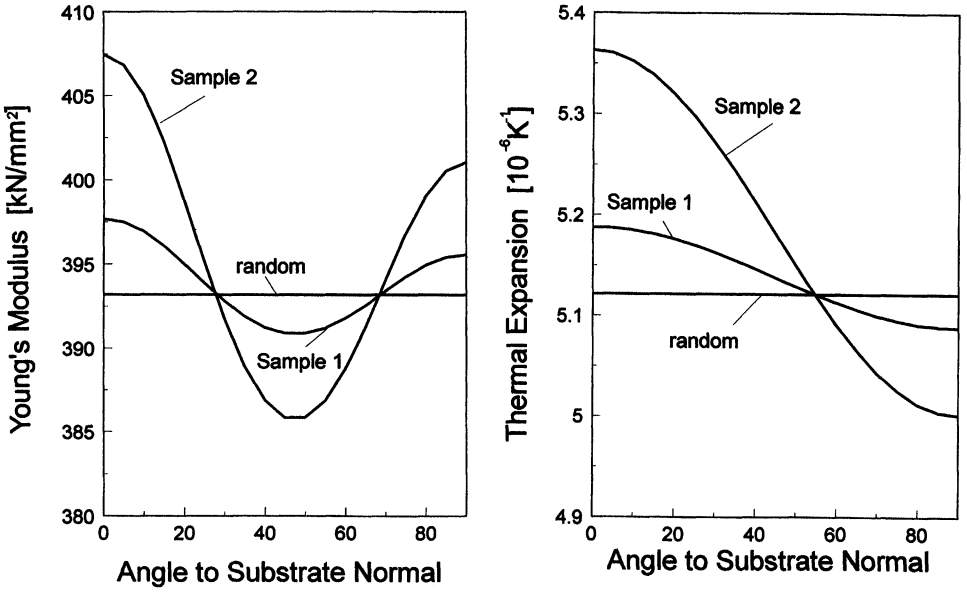

Figure 22 Second and fourth-rank properties of Al_2O_3 for two different experimentally determined textures according to Table 5 a) Young's modulus b) thermal expansion

leads to an expected texture dependence of ~3% as it may be seen in Figure 18. Also in this figure, materials with different structural properties, i.e. grain size and grain boundary phases, are considered together. Hence, the rather wide spread about the interpolating line may easily be understood.

MODEL CALCULATIONS OF PHYSICAL PROPERTIES

In order to estimate the values of physical properties to be expected on the basis of single crystal properties and the texture, the orientation dependence of second and fourth rank tensor properties in textured materials was considered (Park *et al.*, 1993). The following expressions are thus obtained

$$\bar{t}(\alpha) = \tfrac{1}{3}(2t_{11} + t_{33}) + \tfrac{4}{15\sqrt{10}}(t_{33}-t_{11})\,\bar{P}_2(\alpha)\cdot C_2^{11} \qquad \text{second rank} \qquad (11)$$

$$\langle E(\alpha)^{-1}\rangle = \tfrac{1}{15}S_0 + \tfrac{2\sqrt{10}}{525}\,S_2 C_2^{11}\cdot \bar{P}_2(\alpha) + \tfrac{8\sqrt{2}}{945}S_4\cdot C_4^{11}\bar{P}_4(\alpha$$

$$\left.\begin{array}{llllll} S_O = & 8S_{11} & +3S_{33} & +4S_{13} & +2S_{44} \\ S_2 = & -8S_{11} & +6S_{33} & +2S_{13} & +S_{44} \\ S_4 = & S_{11} & +S_{33} & -2S_{13} & -S_{44} \end{array}\right\} \text{fourth rank} \qquad (12)$$

where $C_\lambda^{\mu\nu}$ are the texture coefficients. The axial symmetry of the texture expresses itself in the fact that only the value $\nu = 1$ occurs which corresponds to that symmetry. The

t_{ij} are the components of the considered second rank tensor e.g. thermal expansion. The S_{ij} are the elastic compliances and $\bar{P}_\lambda(\alpha)$ are normalized Legendre polynominals. For model calculations, it is useful to consider also "ideal" textures with a preferred orientation $g = \{\varphi_1 \phi \varphi_2\}$ and Gaussian spread with the spread parameter ω about it. The texture coefficients of such textures can be expressed by

$$C_\lambda^{\mu\nu} = \frac{exp\{-\frac{1}{4}\lambda^2\omega^2\} - exp\ \{-\frac{1}{4}(\lambda + 1)^2\ \omega^2\}}{1-exp\ \{-\frac{1}{4}\omega^2\}} \cdot \dddot{T}_\lambda^{\mu\nu}\ (\varphi_1 \phi \varphi_2) \tag{13}$$

(see e.g. Bunge 1993)
Assuming experimental values of the elastic constants S_{ij} of Al_2O_3 (S_{11} = 2.380 *TPa*, S_{13} = –0.380 *TPa*, S_{33} = 2.191 *TPa*, S_{44} = 7.030 *TPa*) and of thermal expansion ($t_{11} = 5.5 \cdot 10^{-6}$, $t_{33} = 6.9 \cdot 10^{-6}$) the property curves for some model textures were calculated Figure 21. Thereby it was assumed that the c-axis forms the angles 0° (basal texture), 45° and 60° (conical textures), 90° (axial texture) with the substrate normal direction with the spread width $\omega = 0°$ and $0° \leq \varphi_1, \varphi_2 \leq 360°$. They span the possible range of property curves for textures substrates. Furthermore, Figure 22 shows Young's modulus and thermal expansion for two selected substrates with the values specified in Table 5. These values fall into the range shown in Figure 21.

Table 5 Textural parameters of some investigated samples

	f_{max}	C_2^{11}	C_4^{11}
sample 1	3.55	0.727	0.782
sample 2	9.49	2.658	2.500

DISCUSSION OF THE RESULTS

In this paper texture formation in Al_2O_3 substrates and the influence of textures on some physical properties of the polycrystalline materials was studied.

The substrates were produced from raw materials i.e. alumina powders from different sources, having different properties, particularly particle size and shape and their statistical distribution. These properties could be modified, to some extent, by materials processing.

It followed a green forming process which could be either dry or wet. This process leads to a green texture which must be due to rigid rotation of particles since no other orientation changing physical process can be assumed in this production step. The used powders consisted of particles which were either single crystals or polycrystalline agglomerates. Furthermore, the single crystals (as well as the crystallites in the agglomerates) could have well developed crystallographic shapes. In the studied cases these were platelike shapes with the plate parallel to the crystallographic basal plane. Also needle shapes may be considered with the needle axis parallel to the c-axis, but particles of this shape were not used in the present investigations.

During green forming, the particles assume some degree of preferred orientation. This must be due to mechanical torque forces acting upon them. As such, the following must be taken into consideration

- Forces excerted by neighbouring grains which try to align the short axis parallel to the compression direction and the long axes parallel to elongating directions.
- Surface tension in a liquid which tries to align the long dimensions of a particle parallel to the surface.
- Dynamical forces in a flowing liquid.

Generally speaking, the following two conclusions can be drawn about the action of these processes:

- The tendency to orientation will be the stronger the greater the particle aspect ratio is.
- The tendency to orientation will be the stronger the bigger the particle is.
- A tendency to orientation must also be assumed for particle agglomerates as some net-effect of the agglomerated particles.

The green textures observed after dry pressing and calandring must be due to rigid particle interaction alone. The green textures after slurry casting must be formed by all three processes i.e. by rigid interaction of particles in the slurry, by surface tension, and by dynamic forces as was concluded from Figure 5 with and without streaking the slurry. It may be assumed that the same kinds of forces also act during the "burn-out" period of the polymer binder just before sintering. This may account for the factor q in eq(4) which was, however, always very near to unity. This effect was not yet further studied. There were also indications for the three mentioned tendencies according to the properties of the powder particles resulting in strong differences in the green textures as shown in Figure 14, although this could not yet be quantified since the shape-size distributions assumed in Figure 23 were not yet quantified. Nevertheless, the experimental results seem to be in good qualitative agreement with the above principles, which may be illustrated in the schematic diagram Figure 23. Particles with distinct shapes lead to green textures which are the stronger, the bigger the particle. Equiaxed particles or aggregates remain nearly random oriented.
The second production step is sintering. Here the following stages must be distinguished:

- Elimination of pore volume by diffusion without grain growth.
- Formation of a second phase which may be liquid or glassy solid.
- Grain coarsening by diffusion through the grain boundary or the grain boundary phase.

Evidence was obtained that the texture changes during sintering are mainly based on this latter effect. If this is accepted, then the principles of continuous grain growth known from many investigations in a great number of materials as well as from theoretical model calculations can also be applied to texture development during sintering. These are particularly a square-root law for the time dependence and a Boltzmann factor for the temperature dependence. The growth rate factor must contain boundary mobility and driving force and the latter one must be proportional to the total boundary area. This is expressed in the formula eq(4) which was verified quantitatively with respect to the time and temperature dependence. Also qualitative agreement between model and experiment was found with respect to the total boundary area estimated from surface area measurements of the used powders (Bunge *et al.*, 1991, Bunge *et al.*, 1994, Huber and Krahn 1993, Böcker *et al.*, 1993).

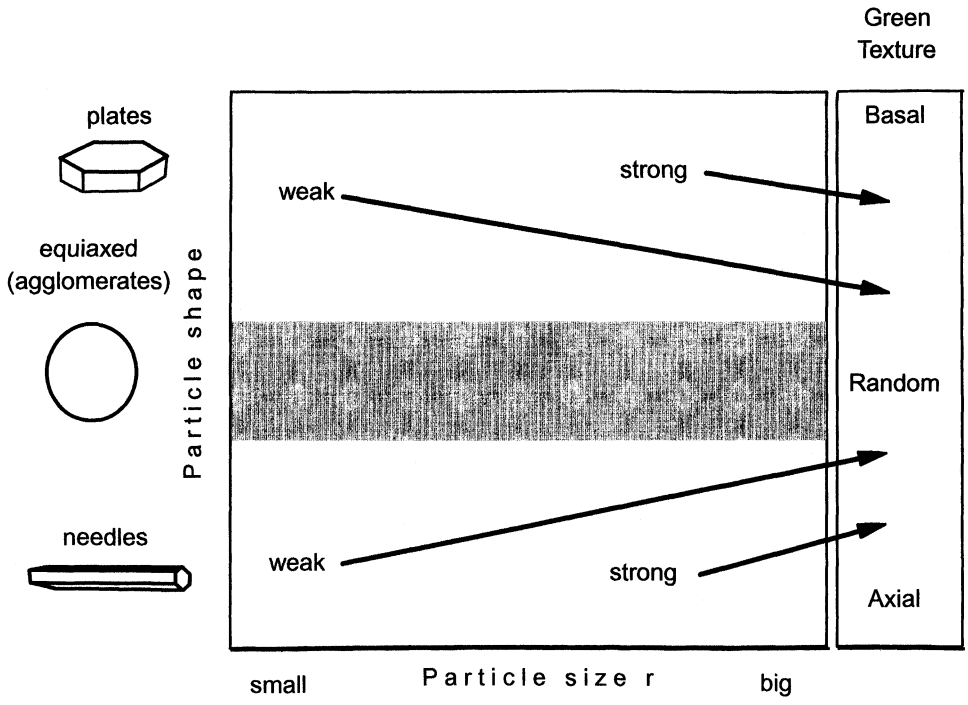

Figure 23 Schematic representation of green texture formation depending on particle size and shape. The arrows indicate regions in the size-shape field from which strong or weak green textures are to be expected

An equation of the type eq(4) is to be expected for the average grain size during grain growth. If we want to apply it to the texture, then a relationship between grain size and texture is required which was experimentally observed in Figure 11. In the theories of continuous grain growth of textured materials the actual size of a particular grain must be compared with a critical size which may be orientation dependent. Hence, a grain bigger than the critical size will grow, if it is smaller than that, it will shrink. The critical size is determined by the whole size distribution of all grains and the orientation of the growing one. The critical size will thus move to greater grain sizes during the growth process as is also indicated in Figure 24. Hence, strictly speaking the "sintering factor" S plotted in Figure 14, 15 depends in a sophisticated way on the complete orientation-size distribution of Figure 24 and that in turn depends on the shape-size distribution of Figure 23. All this is summarized into the microstructural factor p in eq(4), which is, however, not yet further specified in the present study. (This factor has the meaning of an average inverse boundary velocity in the aggregate).

If grain size changes over a very wide range then this factor p should also change. Then deviations from the time and temperature dependences according to eq(4) must be expected. In fact, however, the changes of grain size considered in the present study did not exceed the factor 3 (see Figure 11) and also the sintering factor S, Figure 14, 15, did not exceed this value. Hence, the factor p in eq(4) can be assumed to be nearly constant within these ranges.

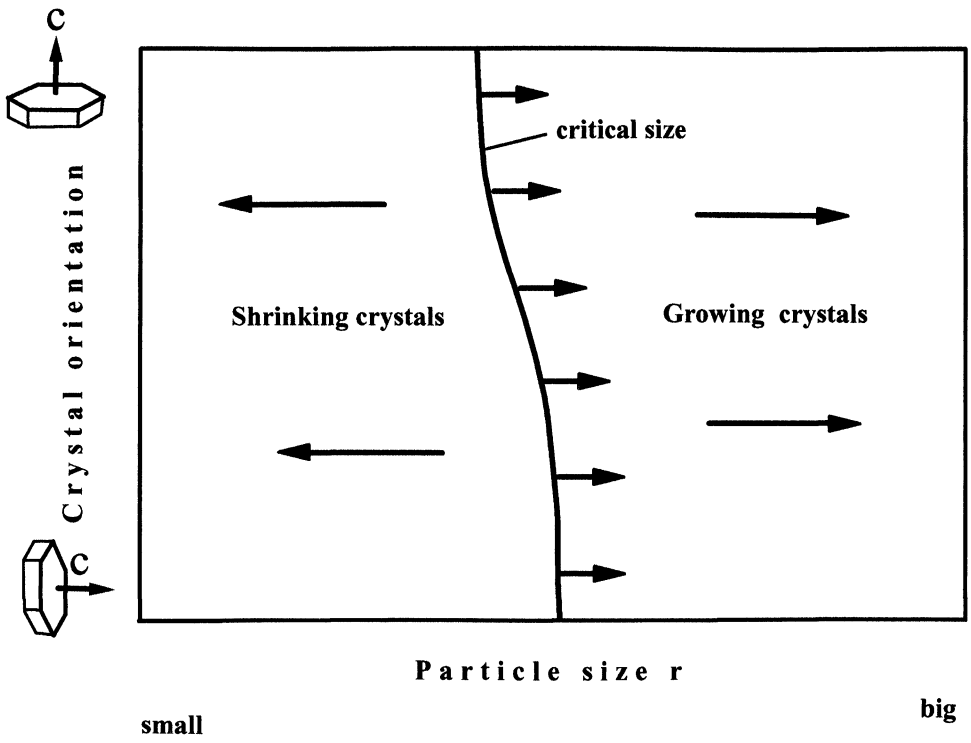

Figure 24 Growth and shrinkage of crystallites during continuous grain coarsening (sintering) depending on grain size and orientation and on the orientation dependent critical grain size

In Figure 13b the Arrhenius plot showed two regions with two different activation energies. Though, it must be mentioned once more, that the low-temperature region is based on the small difference between the texture at temperature T and one extrapolated to the beginning of grain growth. Hence, these values must be considered with a large error limit. Nevertheless, indications of these two regions could be seen in several test series. Hence, one may assume that the two regions are real. It is known that the added sintering aids facilitate sintering. That is the reason why they are added. There is also evidence that this is due to a liquid grain boundary phase the melting point or glass transition temperature of which depends on composition, i.e. on the used sintering aids. In the present study S_iO_2, MgO and CaO were used in varying compositions. The melting points of the so obtained glass phases are not exactly known, they are, however, in the range of 1400°C. It may thus be assumed that the transition temperature Tc in Figure 13 b and Table 3 is correlated with the melting temperature of the grain boundary phase. As is seen in Table 3 the activation energy in the high temperature region varies from one material to the other which was, however, not further evaluated in the present study. In any case, the observed activation energies were in the order of magnitude of volume diffusion in Al_2O_3 (see e.g. Salmang and Scholze 1982). The activation energy of the low temperature region is smaller than that of the high temperature region. Hence, another diffusion mechanism must be responsible in

this region. Since, however, the accuracy of the results in this region was too low, further, more accurate, measurements are required in order to draw further conclusions.

In the present study also physical properties of the final sintered materials were considered. All properties which are anisotropic in the individual crystallite are influenced by the texture of the material in three different ways illustrated in Figure 25.

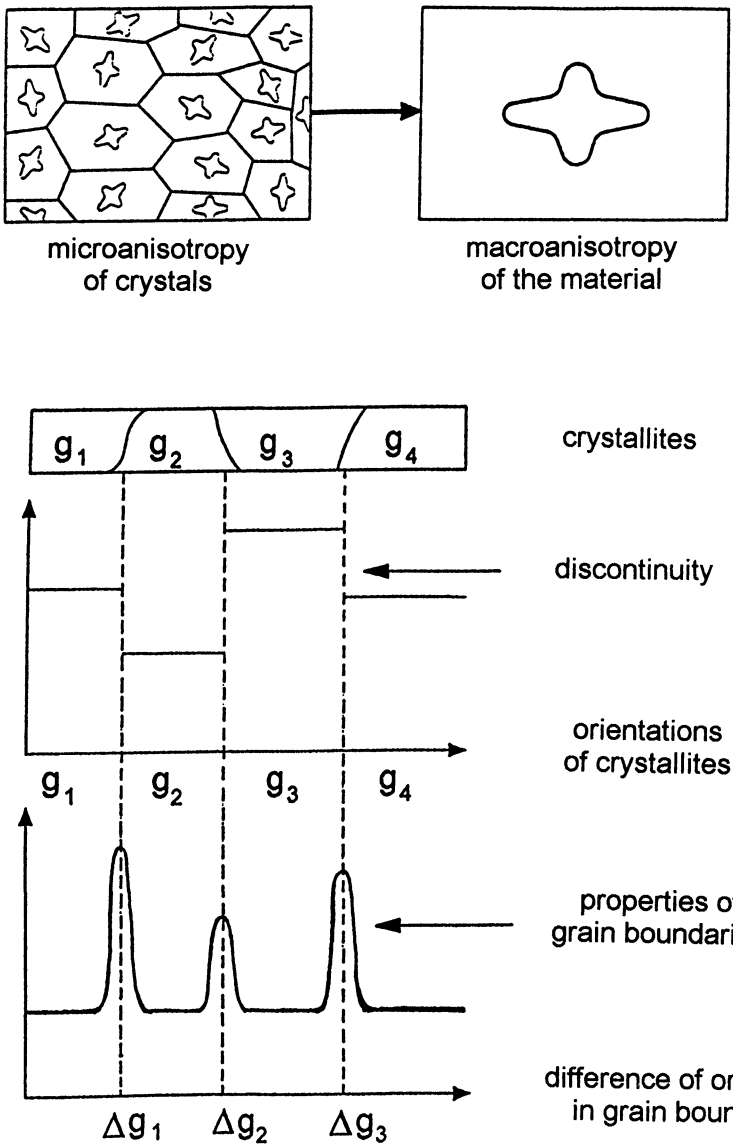

Figure 25 Three effects depending on crystal orientation in polycrystalline materials a) Macroanisotropy b) Microdiscontinuity c) Grain boundary properties

- The microscopic anisotropies of the crystallites are averaged with the texture as the weight function to the macroscopic anisotropy
- In the grain boundaries the values of anisotropic properties may change discontinuously as a consequence of the discontinuous change of orientation accross the boundary. This effect depends on misorientation Δg accross the boundary and, as a whole, it depends on the misorientation distribution function MODF which is related to the texture (although it is not completely fixed by the texture).
- Finally, a third effect must also be considered which is also related to individual misorientation and to the MODF. This is deviating properties in the grain boundaries. In the present materials the deviating grain boundary phases may be subsumed also under this point.

All three effects, influenced by the texture, are shown in Figure 25. As it was shown, all three effects must be taken into consideration in order to understand the texture dependences of the three mechanical poperties investigated in this study:

Macroanisotropy of thermal expansion in Al_2O_3 was assumed to be responsible for half of the texture dependence of thermal cycling resistance in Figure 17.
Macroanisotropy of Young's modulus was assumed to explain the (small) slope of the bending fracture curve Figure 18.
Microdiscontinuity of thermal expansion is assumed to be the main reason for the texture dependence of thermal shock fracture in Figure 19.
Grain boundary properties, finally, were assumed to account for the spread in Figure18 and Figure19.

CONCLUSIONS

Based on the experimental results, qualitative conclusions about the mechanisms of green texture formation could be obtained. For the second process - sintering - a quantitative model for texture formation could be developed. The parameters entering this model were not yet quantified in the present investigation. Nevertheless, qualitative estimates were possible. On the basis of these model assumptions, conditions for the formation of strong or weak textures, as well as for textures of different types can be given. Some particular examples are shown in Figure 26 in terms of the particle size-shape distribution illustrated in Figure 23. A small-grain fraction provides the driving force for grain growth. A large-grain fraction will form part of the green texture and will act as "seeds" during grain growth. Hence, the distributions in Figure 26 a, b, c respectively will lead to a strong basal, random, or strong axial texture, respectively. Random texture can also be expected by "compensating" basal with axial textures as is illustrated in Figure 26d. A weak texture may also be expected if there is no fine-grain fraction as in Figure 26e, so that the sintering factor is particularly small.

Which texture is desirable, depends on the purpose for which a material is being used. In many cases, not only one physical property is of interest. Often a whole "spectrum" of physical properties may be interesting, each of which may have a different texture dependence as for example the thermal shock resistance and thermal cycling resistance shown in Figure 17 and Figure 19. It has also been shown that, besides the texture, also other textural quantities such as the misorientation distribution function MODF must be included in the considerations, e.g. by individual orientation analysis.

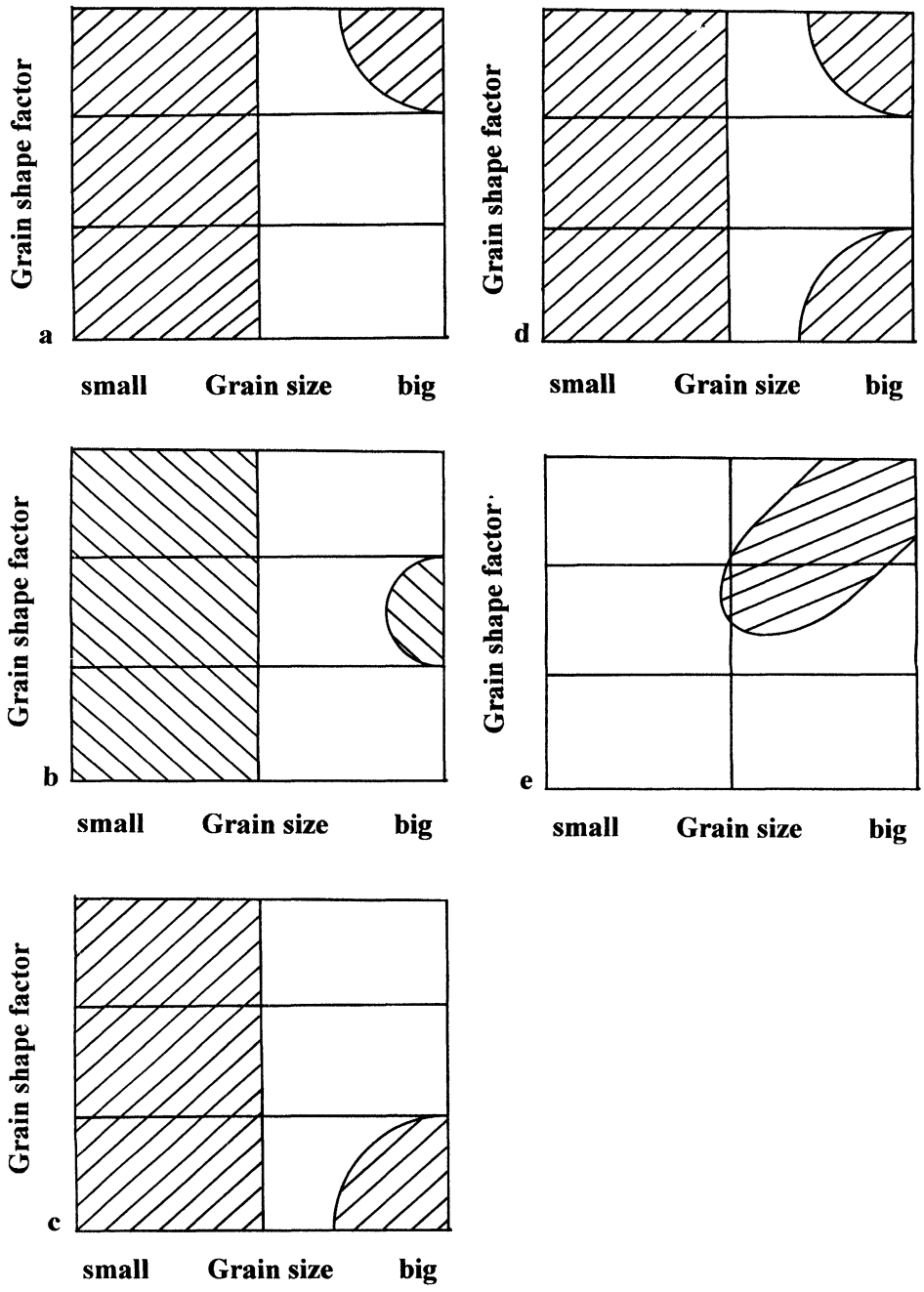

Figure 26 Some examples of grain size-shape distributions leading to particular types of textures a) basal texture b) random texture c) axial texture d) pseudo-random (compensated) texture e) weak (basal) texture

Finally, it is necessary to come to a quantitative model of green texture formation and to provide more quantitative parameters about particle size and shape in order to quantify the model assumptions of texture formation during sintering described in eq(4).

Acknowledgement

The authors gratefully acknowledge support of this project by BMFT under contract 03 M2037. Furthermore, we want to thank Siemens Analytical for the possibilty to carry out the measurements with the $\vartheta - \vartheta$ goniometer.

References

Böcker, A. (1994). Einfluβ von Material und Verarbeitung auf die Texturbildung in Al_2O_3 Substraten Thesis Clausthal.

Böcker, A., Brokmeier, H. G. and Bunge, H. J. (1991). Determination of preferred orientation textures in Al_2O_3 ceramics. *J. Eur. Ceram. Soc.*, **8** 187–194.

Böcker, A., Bunge, H. J., Ernst, J. and Krahn, W. (1993). Texture evolution in Al_2O_3 sheets by grain growth during sintering In: Recrystallization '92, ed. M. Fuentes and J. Gil Sevillano Trans Tech Publications, Switzerland,; 575–578.

Böcker, A., Bunge, H. J., Huber, J. and Krahn, W. (1994). Texture Formation in Al_2O_3 Substrates Journ. of the European Ceramic Society **14** 283–293.

Bunge, H. J. (1993). Texture Analysis in Materials Science. Second Ed. Cuvillier Verlag Göttingen.

Bunge, H. J., Böcker, A., Ernst, J. and Krahn, W. (1991). Einfluβ von Material und Verarbeitung auf die Texturausbildung in Al_2O_3 Substraten. In: Proc. 2. Symp. Materialforschung, Dresden, Bundesminister für Forschung und Technologie, pp. 1823–1833.

Bunge, H. J. and Dahlem-Klein, E. (1993). Model calculations of grain growth by anisotropic boundary energy and mobilty in textured materials. In: Recrystallization '92 ed. M. Fuentes and J. Gil Sevillano. Trans Tech Publications, Switzerland, 299–304.

Bunge, H. J., Böcker, A., Krahn, W. and Ruska, J. (1994). Untersuchung von Einfluβgröβen auf die Texturbildung bei foliengegossenen Al_2O_3. Substraten. Symposium Materialforung - Neue Werkstoffe. Würzburg PLR Jülich 839–840.

Dimarcello, F. V., Key, P. L. and Williams, J. C. (1972). Preferred orientation in Al_2O_3 substrates. *J. Am. Ceram. Soc.*, **55** 509–514.

Huber, J. and Krahn, W. (1992). Untersuchung der Texturbildung in Al_2O_3 Substraten. Final Report BMFT project 03 M 2037 (0992).

Klein, H., Waibel, B., Martin, W., and Bunge, H. J. (1989). Reliability of copper metallized Al_2O_3 substrates during thermal cycling as a consequence of preferred orientation (texture). In: Joining Ceramics, Glass and Metal. ed. W. Kraft. DGM Informationsgesellschaft Oberursel, 285–290.

Nakada, Y and Schock, T. L. (1975). Surface texture formation in Al_2O_3 substrates. *J. Am. Ceram. Soc.*, **58** 409–412.

Park, N. J. Klein, H. and Dahlem-Klein, E. (1993). Program System: Physical Properties of Textured Materials. Ed. H. J. Bunge, Cuvillier Verlag Gottingen.

Salmang, H. and Scholze, H. (1982). Keramik. Springer Verlag Berlin.

Waibel, B., Martin, W., Fett, T. and Bunge, H. J. (1990). Texture correlated cycliy fatigue of alumina substrates Proc. I. CIMTEC, Montecatini B 1.4-L05.

Winkelmann, K., Göbel, O., Nikkilä, A. P., Vuorinen, P., Mäntylä, T. and Zschech, E. (1994). Einfluβ von Additiven auf das Sintern, das Gefüge und die mechanischen Eigenschaften von Al_2O_3-Keramik. Metall **48** 382–387.